Exploring the Impact of Inlet Air Velocity Variations on Heat and Mass Transfer in a Tea-Focused Fluidized Bed Dryer: A Comprehensive Numerical Analysis

Yohana, Eflita
Department of Mechanical Engineering, Diponegoro University

Tauviqirrahman, Mohammad
Department of Mechanical Engineering, Diponegoro University

Yusuf Luqmanul Hakim
Department of Mechanical Engineering, Diponegoro University

Mohamad Endy Yulianto
Department of Chemical Engineering Vocational School, Diponegoro University

他

https://doi.org/10.5109/7236861

出版情報：Evergreen. 11 (3), pp.2175-2185, 2024-09. Interdisciplinary Graduate School of Engineering Sciences, Kyushu University, Japan
バージョン：

Exploring the Impact of Inlet Air Velocity Variations on Heat and Mass Transfer in a Tea-Focused Fluidized Bed Dryer: A Comprehensive Numerical Analysis

Eflita Yohana[1,*], Mohammad Tauviqirrahman[1], Yusuf Luqmanul Hakim[1], Mohamad Endy Yulianto[2], Ridho[1], M. Farkhan H. Dwinanda[3], Kwang-Hwan Choi[4]

[1]Department of Mechanical Engineering, Diponegoro University, Jl. Prof. Soedarto, S.H., Semarang, 50725, Indonesia

[2]Department of Chemical Engineering Vocational School, Diponegoro University, Jl. Prof. Soedarto, S.H., Semarang, 50725, Indonesia

[3]Chemical Engineering, The University of Queensland, St Lucia QLD 4072, Queensland, Australia

[4]College of Engineering, Pukyong National University, 365 Sinseon-ro, Nam-gu, Busan 608-739, Korea

*Author to whom correspondence should be addressed:
E-mail: eflitayohana@live.undip.ac.id

(Received January 25, 2024: Revised June 16, 2024: Accepted June 21, 2024).

Abstract: Fluidized bed dryer is used for the drying process because it has a high rate of mass and heat transfer. The purpose of this study is to analyze heat and mass transfer caused by the inlet velocity of airflow. CFD was used to study hydrodynamic phenomena in modeling fluidized bed dryers. This study used Eulerian-Eulerian (gas-solid) multiphase approach and used laminar flow to examine the phenomenon of mass and heat transfer. The simulation varied the inlet velocity of air at 1.6, 1.8, 2.1, and 2.3 m/s with a constant temperature at 403 K. At the lowest velocity, 1.6 m/s, the solid-gas heat transfer coefficient is 344.2 $W/m^2.K$, and the coefficient of the mass transfer is 0.98×10^{-7}, while at the highest velocity, 2.3 m/s, the solid-gas heat transfer coefficient is 353.3 $W/m^2.K$ and the coefficient of the mass transfer is 2.55×10^{-7}. The results of the analysis show that the tea drying rate will be higher if it has a high velocity.

Keywords: fluidized bed dryer; CFD; drying; inlet velocity

1. Introduction

Drying constitutes a pivotal process within numerous industries, holding significant importance. Drying a solid object is useful to reduce or remove moisture into an acceptable value. Many agricultural products need to be dried to reduce their moisture content to reach a humidity point that is safe for storage[1]. Even in some agricultural products, for example, tea, the drying process is also important not only to reduce the moisture content but also to improve the quality of the aroma of the product[2]. One of the many tools that are usually used in the process of drying is a fluidized bed dryer (FBD). Fluidized bed dryers are broadly applied in industries such as mining and pharmaceutical fields. The utilization of FBD is common in drying of solid substances, primarily owing to its ability to process materials with a wide particle size distribution[3], and its notable efficacy in mass and heat transfer[4], thereby contributing to an overall drying time reduction. This study centers on the drying process of tea particles, which are conceptualized and modeled as solid particles. There have been many previous studies discussing tea drying methods, one of which is the tea drying method proposed by Gunawan et al.[5], which utilizes geothermal heat and zeolite in the withering tea process. In the context of drying tea leaves, FBD is employed to extract moisture or water from the tea leaves, facilitating the drying process. It is imperative to establish appropriate FBD parameters to ensure that the leaves achieve sufficient dryness while preserving the quality of taste, color, and aroma[6].

In contrast to other applications of Fluidized Bed Dryers (FBD), the drying of food ingredients, specifically tea in this study, necessitates careful consideration of its organic composition. Consequently, the drying temperature was restricted to not exceed 403 K, aiming to preserve the organic constituents in tea, including catechin, and also keep the liquoring quality of the tea[7]. But still try to keep the tea at a good level of dryness for storage purposes.

Although Fluidized Bed Dryers (FBD) are commonly used for drying tea leaves, there is a need for simulation models to design operational settings and control systems[8], providing a deeper understanding of the FBD system in the context of tea leaf drying. Among the significant variables influencing FBD settings, the velocity value stands out. Consequently, this research aims to conduct simulations of the FBD system, specifically exploring variations in inlet air speed values.

A great perceptivity of heat transfer and flow characteristics is needed to optimize the control and analysis of FBD. The fluidization quality in FBD is subject to influence from various factors, including geometry, operating conditions, and the physical characteristics of solid particles. Alterations in these parameters can result in hydrodynamic changes within the system[9]. Many factors affect the bed and the wall heat transfer, in example, the particle size and speed of airflow[10]. Bakshi et al.[11] have researched the impact of the coefficient of specularity using the Eulerian-Eulerian model on the hydrodynamics of FBD in a three-dimensional model. A comparative analysis between the simulation outcomes and experimental findings is conducted to ascertain their respective effects. Schmidt and Renz[12] perform numerical studies of heat transfer in FBD walls and solid particles. Different models for solid-solid thermal conductivity, using the conventional approach and kinetic theory for granular flow (KTGF). Dong et al.[13] simulate multiphase flow dynamics within FBD using the Eulerian-Eulerian model. They found that the characteristics of the flow and the heat transfer that occur in the FBD were impacted by the effect of different tube shapes and effective thermal conductivity. In this study, granular modeling of particles in tea particles was adopted to determine the heat transfer between particles with the wall[14]. The governing equations for the two-fluid models were completed and solved employing the KTGF. This theory assumes that the random movement of the particles caused by the impact is parallel to the thermal movement of gas molecules[15].

To analyze the heat transfer between the bed and the wall, a numerical method is needed and interacts with the fluidized bed. CFD simulation was chosen because it makes it easier for researchers to be able to determine the characteristics of a model without having to make it directly. CFD simulations are commonly used to compare with actual conditions of tools or machines, such as research conducted by Bahar et al.[16] in their research comparing actual and simulated air conditions in a chamber. Computational Fluid Dynamics (CFD) has been formed as an excellent approach to simulating fluid and systems of multiphase[17]. CFD simulation can also provide a much deeper view of understanding gas-solid flows in a fluidized bed dryer and provide more detailed data down to a very small size that experiments cannot provide[18]. In this research, the Eulerian-Eulerian approach employed to study heat transfer between the bed and the wall in different operations, such as the velocity of airflow, drag model, and particle diameter size. The KTGF was employed to estimate the properties of solid particles, such as viscosity, shear viscosity, and pressure[19]. This study analyzes the results of heat transfer and mass transfer in the airflow in the fluidized bed using numerical methods. The drag model used in the simulation is Syamlal-O'Brien because it is suitable on high fluidization rate[20]. The Syamlal-O'Brien drag model was also found to have high accuracy among several other drag models that can be used in gas-solid flow hydrodynamic modeling for fluidized beds, such as Wen-Yu and Gidaspow drag model[21].

Three-dimensional models provide better results and simulations that approach actual conditions compared to two-dimensional models. There are lots of uses that can be generated by simulating the operating parameters of the fluidized bed dryer; for example, in the velocity parameter, we can find out what the minimum velocity value is for fluidization to occur on the fluidized bed dryer by using CFD simulations as done by Gosavi et al.[22], besides that, we can find out the fluidized bed dryer overall flow characteristics as was done in this study which tries to provide variations in the inlet air velocity to see the influences of the flow formed on the FBD.

The purpose of this study was to present the results of a three-dimensional model numerical simulations so that the data can be obtained in the form of graphs to find the effect of variations in air velocity on mass and heat transfer that occur in FBD. Most of the studies that have been done previously focused on finding the minimum fluidization velocity; there is still no other study that specifically simulates how the inlet air velocity affects the value of the heat and mass transfer coefficient in a FBD. For this reason, this study will be discussed and analyzed specifically concerning variations in inlet air velocity to heat and mass transfer values. Studies varying the air inlet velocity are required to be able to demonstrate the flow of gas-solid characteristics[23]. The inlet air temperature will be maintained as a constant parameter throughout the simulation runs. This approach allows for a clear observation of the impact of variations in inlet air velocity, without any confounding influence from changes in incoming air temperature. Even though this is something that is quite important and fundamental to see how one of the main parameters of the fluidized bed dryer, which is inlet air velocity, can affect the overall flow characteristics in the fluidized bed dryer, this study will analyze heat and mass transfer, this is discernible through the examination of the solid volume fraction within the fluidized bed dryer, a process facilitated by the Computational Fluid Dynamics (CFD) methodology, and analyze how the variations in inlet flow velocity will affect on fluidization phenomena in a fluidized bed dryer.

2. Methodology

2.1 General Equations

In this study, fluidized bed dryers were carried out using the method produced by Hamada Mohammed Abdelmotalib and Im[20]. CFD was used to study hydrodynamic and counterfeit phenomena in 3D gas-solid modeling fluidized bed dryers. The present investigation employs the Eulerian-Eulerian (gas-solid) multiphase methodology, utilizing laminar flow to scrutinize the hydrodynamic and heat transfer phenomena. The use of laminar flow model in this investigation is justified by the fact that the maximum Reynolds number of the particles is determined to be 83.10, thereby classifying the flow as laminar. While laminar flow is not conventionally employed in Fluidized Bed Dryer (FBD) studies, the decision is supported by Abdelmotalib and Im's research. Their work demonstrated the reliability of employing laminar flow models in studying FBD under conditions characterized by relatively low velocities and particles of substantial weight.

Within the Eulerian-Eulerian framework, both solid and gas phases are delineated employing a continuous mathematical equation approach, each accompanied by a corresponding conservation equation. The CFD software is deployed for the simultaneous resolution of energy, momentum, and mass equations. The derivation of phase properties in a granular flow is facilitated through the application of kinetic theory. The continuity equations for the gas phase (g) and solid phase (s) are expressed as Eq. 1 and Eq. 2, respectively.

$$\frac{\partial}{\partial t}(\rho_g \varepsilon_g) + \nabla(\rho_g \varepsilon_g v_g) = 0 \quad (1)$$

$$\frac{\partial}{\partial t}(\rho_s \varepsilon_s) + \nabla(\varepsilon_s \rho_s v_s) = 0 \quad (2)$$

Total volume fraction of gas, ε_s, and solid, ε_g, is equal to 1. ρ is density and v is velocity. Eq. 3 and Eq. 4 show the equation of momentum for solid and gas phases.

$$\frac{\partial}{\partial t}(v_g \rho_g \varepsilon_g) + \nabla(v_g v_g \rho_g \varepsilon_g) = -\nabla P_g \varepsilon_g + \rho_g \varepsilon_g g + \nabla \tau_g + \alpha_{gs}(v_s - v_g) \quad (3)$$

$$\frac{\partial}{\partial t}(v_s \rho_s \varepsilon_s) + \nabla(v_s v_s \varepsilon_s \rho_s) = -\varepsilon_g \nabla P_g - \nabla P_s + \nabla \tau_s + \varepsilon_s \rho_s g + \alpha_{gs}(v_g - v_s) \quad (4)$$

In the equation of momentum, α_{gs} is the interphase drag exchange coefficient given by the Syamlal-O'Brien drag model, g is the acceleration of gravitational, τ is the Reynolds tensor stress, and the force of interaction (buoyancy and tensile) describes the transfer of momentum between the gas and solid phase indicated by Eq. 5.

$$[-\varepsilon_s \nabla P_g + \alpha_{gs}(v_g - v_s)] \quad (5)$$

Where P_g is the pressure on the fluidized bed. The energy equations for the gas phase and solid phase are expressed as Eq. 6 and Eq. 7, respectively.

$$\frac{\partial}{\partial t}(H_g \rho_g \varepsilon_g) + \nabla(v_g H_g \rho_g \varepsilon_g) = \nabla(k_g \varepsilon_g \nabla T_g) - \delta_v (T_g - v_s) \quad (6)$$

$$\frac{\partial}{\partial t}(H_s \rho_s \varepsilon_s) + \nabla(v_s H_s \rho_s \varepsilon_s) = \nabla(k_s \varepsilon_s \nabla T_s) + \delta_v (T_g - v_s) \quad (7)$$

H is the enthalpy, k is thermal conductivity, and δ_v is the volumetric interphase heat transfer coefficient. Reynolds number is a value for determining the fluid flow type in FBD. For particles (solid), Re_s can be calculated using Eq. 8.

$$Re_s = \frac{\rho_s d_s \left| v_s - v_g \right|}{\mu_g} \quad (8)$$

d_s is the diameter of the particle, and μ is the viscosity of the fluid flow. A constitutive equation is employed to augment the equation, wherein the tensor stress of the solid pahse, denoted ad τ_s, is defined according to Eq.9.

$$\tau_s = \varepsilon_s \mu_s (\nabla v_s + \nabla v_g^{\,T}) + \varepsilon_s (\lambda_s - \frac{2}{3}\mu_s) \nabla v_g I \quad (9)$$

Where I is the inertia and μ_s is the solid phase shear stress, given according to Eq. 10.

$$\mu_s = \mu_{s,col} + \mu_{s,kin} + \mu_{s,fr} \quad (10)$$

Eq. 11 shows the particle collision viscosity, $\mu_{s,col}$.

$$\mu_{s,col} = \frac{4}{5}\varepsilon_s \rho_s d_s g_{0,ss}(1 + e_{ss})\left(\frac{\theta_s}{\pi}\right)^{1/2} \quad (11)$$

The equation used to find the pressure drop is Eq. 12 as follows,

$$\Delta P.S = (SL_{mf})(1 - \varepsilon_{mf})(\rho_p - \rho_f)g \quad (12)$$

L_{mf} represents fluidized bed height and ε_{mf} is the fraction of volume. The pressure of the solid particles in the fluidized bed has its own pressure, which is shown in Eq.13. Pressure of the particle (solid pressure) is characterized as a function of kinetic time (ε_s, θ_s, ρ_s) and ($2\rho_s$ $(1+e)$ $\varepsilon_s^2 g_0 \theta_s$) states the effect of particle collisions.

$$p_s = \varepsilon_s . \rho_s . \Theta_s + 2\rho_s (1+e) \varepsilon_s^{\,2} g_0 \, \Theta_s \quad (13)$$

In the specific scenario granular flow, pressure of the particle can be independently determined, with the coefficient of restitution for temporary colliding particles as a radial distribution function represented by e. Term g_0 is the radial distribution which state according to Eq.14.

$$g_0 = \frac{(1+2.5\varepsilon_s + 4.59\varepsilon^2 + 4.52\varepsilon^3)}{(1-(\frac{\varepsilon_s}{\varepsilon_{smax}})^3)} \quad (14)$$

The Nusselt number, a dimensionless parameter governing heat transfer within a fluid flow, is expressed by Eq.15, which is provided by Gunn[24]. This equation is commonly used to estimate the Nusselt number in a multiphase case, like in this study.

$$Nu = \frac{\delta_{as} d_s}{k_g} = (7 - 10\varepsilon_a + 5\varepsilon_a{}^2)(1 + 0.7\,\mathrm{Re}_s{}^2\,\mathrm{Pr}^{0.33}) + (1.33 - 2.4\varepsilon_a 1.2\varepsilon_a{}^2)\,\mathrm{Re}_s{}^{0.7}\,\mathrm{Pr}^{0.33} \quad (15)$$

Where Pr is the Prandtl number of the air, which is given in Eq.16, and δ_{as} is the gas-solid interphase heat transfer coefficient. In this research, the heat transfer coefficient values are derived from the correlation provided by Gunn[24], a commonly employed approach in multiphase calculations.

$$\mathrm{Pr} = \frac{C_{pa}\mu_a}{k_a} \quad (16)$$

Sherwood number is a number that shows the mass transfer operation of a flow. The equation given by Vepsäläinen[25] is used To find the Sherwood number in this study, which can be seen in Eq. 17.

$$Sh = 2\alpha + 0.69\,\mathrm{Re}^{1/2}\,Sc^{1/3} \quad (17)$$

The diffusivity coefficient is determined according to the Eq.18 if the air temperature falls within the range of 280 K < T < 450 K.

$$D_{gs} = 1{,}87 \times 10^{-10 \frac{T^{2,072}}{p}} \quad (18)$$

The obtained diffusivity coefficient allows for the determination of the Schmidt number (Sc), a dimensionless quantity defined as the ratio of momentum diffusivity (kinematic viscosity) to mass diffusivity. It is utilized to characterize fluid flow, and its calculation is governed by the following equation.

$$Sc = \frac{v}{D} = \frac{\mu}{\rho D} \quad (19)$$

Due to the laminar flow conditions employed in this research, the mass transfer coefficient, h_{mass}, is calculated using the Eq. 20.

$$h_{mass} = \frac{ShD_{gs}}{L_c} \quad (20)$$

All of these governing equations, along with another additional equation that closes, forms the basis of calculations that will be executed on the elements or grids of the model to later produce the values needed in this study. All of the governing equations are needed to be used in the calculation process to find the heat and mass transfer coefficient that occurs in the FBD.

2.2 CFD Model

The geometry of the FBD was obtained from the cross-section of the chamber in a tube-shaped fluidized bed dryer. The design of the fluidized bed dryer model used in this study is shown in Fig. 1. The dimensions of FBD are: height H = 500, width D = 24, length L = 90, and particle height (h particle) = 176. All dimensions are in millimeters.

The multiphase model was set to Eulerian with two Eulerian phases, and the fraction of volume parameters formulation was set to implicit. The Eulerian-Eulerian method in the simulation uses one main phase, namely air, but this air phase is divided into two types. The first type is as air, and the second one is as solid, with its material properties are; gas density = 1.2 kg/m^3, particle density = 2520 kg/m^3, initial solid packing = 0.6, diameter of particle = 560 µm, fluidization gas temperature = 403 K, initial particle temperature = 298 K, the thermal conductivity is 0.25 W/m.K for the particle, and 0.025 W/m.K for the air. The particle specific heat is 800 J/kg.K, and 1005 J/kg.K for the air. Based on the initial speed that the fluid can enter the steamer chamber, so, the air velocities in velocity inlet boundary conditions setup which used are 1.6, 1.8, 2.1 and 2.3 m/s with 403 K temperature. The solid phase has no velocity, and the temperature value is 298 K.

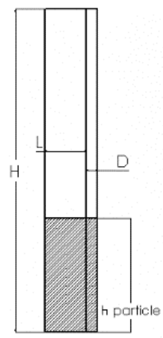

Fig. 1: Geometry of fluidized bed dryer.

For the outlet side, the boundary condition used is pressure outlet, where the pressure value on the outlet side has the same value as the surround atm pressure, so for the air or solid phase, the gauge pressure is set to zero. Wall boundary condition in simulation is considered no heat and stationary wall. The wall on the simulation is also divided into two types, which are the solid and the air phase. For the air phase, a no-slip condition is defined for the wall; for the solid phase, a 0.5 specularity coefficient is defined for the wall. The Syamlal-O'Brien drag model was set in the drag coefficient of phase interaction, and Gunn was used in the coefficient of heat transfer of phase interaction. In this research simulation, the solution method used is second-order upwind discretization for momentum and energy, QUICK for volume fraction, second-order implicit for the transient formulation, and SIMPLE for pressure-velocity coupling. The SIMPLE algorithm is used to realize smooth simulation calculations by simultaneously correcting the pressure and velocity fields[26].

2.3 Grid Generation

Meshing is a process of breaking down a solid model into small parts or elements so that later the boundary settings can be imposed to the meshing results[27]. In CFD simulation, the accuracy of the calculation is influenced by the size of the element[28]. A finer grid or smaller-sized elements in the model contribute to increased accuracy in the obtained results. As a consequence, it requires much more computer calculation power and takes more time than the larger element or grid. Because of that, simulations with variations on the total of elements are needed to make sure that the simulation value from the grid we chose is right and does not rely on the number or size of the elements. The parameter used as a comparison to carrying out the grid test and validation later is the coefficient of the heat transfer value. The element number and the error percentage of the independence grid test are shown in Table 1, and Fig.2 shows the grid generation result.

From Table 1, it is shown that a geometry consisting of 135,000 elements in the simulation results in a minimal error value. Hence, increasing the number of elements is unnecessary, as it would yield negligible differences in results and would not introduce a substantial error (<5%)[28]; then, this element number is chosen for the grid. Hence, this research uses a hexahedral grid with 135,000 elements with a 1.32E-10 maximum skewness result and 0,02% error percentage.

Table 1. Grid independence test result.

Elements	Skewness	h (W/m^2K)	Error (%)
102377	1.32E-10	56.26	-
107646	1.32E-10	73.02	0.30
112574	1.32E-10	81.33	0.11
135000	1.32E-10	82.57	0.02
141312	1.32E-10	88.92	0.08

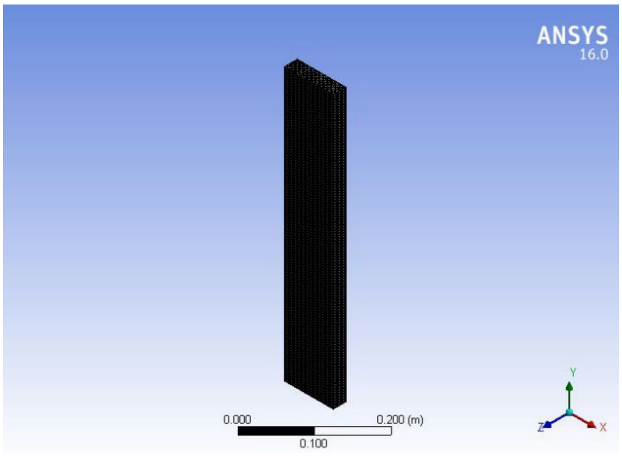

Fig. 2: Hexahedral grid generation result.

2.4 Validation

Results from numerical simulations must be validated with experimental data or other research with similar parameter. The simulation outcomes in this research are juxtaposed to the study conducted by Abdelmotalib and Im[20]. The coefficient of heat transfer on bed-to-wall in the fluidized bed of this study and reference are compared for validation. Figure. 3 shows the error of simulated results. The average of the validation errors found in this study was 0.99%, with the highest error of 1.34% at 1.6 m/s. The maximum deviation between CFD results and validation results which can be accepted must be below 10%[29]. Due to the error that was gained less than 10%, the method in this study can be used for subsequent simulations.

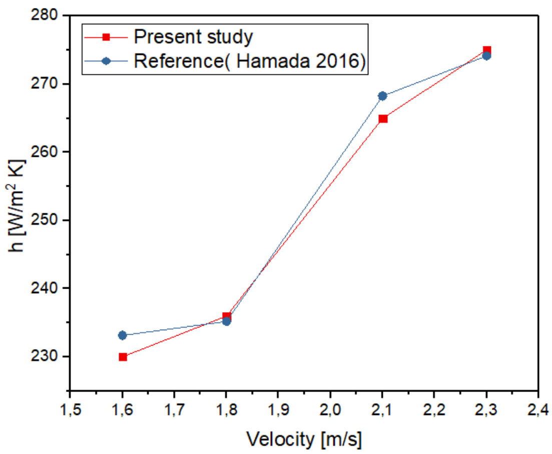

Fig. 3: Validation result.

3. Result and Discussion

The simulation outcomes are the contours of velocity distribution, temperature, solid volume fraction, coefficient of heat transfer, and mass transfer coefficient that are influenced by the inlet velocity variation. This study is not concerned with calculating the minimum velocity, which is the velocity at which the transition between a fluidized bed and a fixed bed state happens[30].

All inlet air velocities used as research variations this time are confirmed to be above the minimum velocity value so that the simulation results can certainly provide a clear picture as a comparison of the flow characteristics that are formed in various inlet air velocity conditions.

3.1 Effect of Velocity Inlet on Solid Volume Fraction

The fluidization process begins when air enters through the distribution plate, which forms microbubbles in large numbers at the bottom of the bed. Then these bubbles merge and form bubbles with larger sizes in the rising process[31]. This rising stage occurs at approximately the initial 0.5 seconds, and this stage is one of the sections that can be considered to see the fluidized bed dryer's performance due to the inlet air velocity variation. In this stage, the axial velocity and diameter of the air bubbles gradually increase[32].

The examination focuses on velocity, temperature, and solid volume fractions distribution to elucidate the dynamics of heat and mass transfer concerning tea particles. Figure 4 and Figure 5 depict the contour plots of volume fraction of the solid at 1.6 m/s. The air temperature is 403 K, and the particle temperature in this condition is 298 K. The size of the particle is 560 µm.

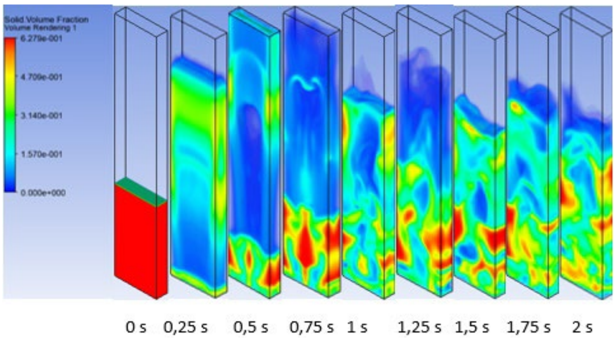

Fig. 4: 3D solid volume fraction at 1.6m/s.

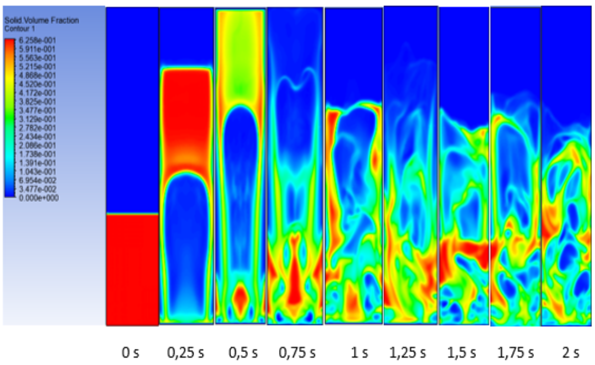

Fig. 5: 2D solid volume fraction at 1.6m/s.

At low velocity, the lifting of solid particles is slower than the lifting of the solid particle at high velocity. This is due to the collision that occurs between the particles increases when the velocity inlet is higher. Thus causing the solid particles to lift quickly. Figure 6 shows the solid volume fraction contour at 1.8 m/s. Compared to 1.6 m/s variation seen in Fig. 5 and Fig. 6, it appears that the increase in velocity resulted in a higher collision and separation effect. It can be seen at 0.25 s. At 1.8 m/s, particles are lifted higher than at 1.6 m/s.

Figure 7 shows the volume fraction of the solid at 2.1 m/s. In Figure 7, it can be seen that at 0.25s, particles have reached the upper limit of the chamber when compared with speeds of 1.6 m/s and 1.8 m/s. Furthermore, particles descending exhibit higher velocities compared to their velocities at the preceding speed. This is due to solid particles have been evaporated faster at 2.1 m/s than at the previous velocity.

In Figure 8, it appears that with the velocity at 2.3 m/s, particles are lifted faster than at other velocity variations. This is due to the momentum resulting at 2.3 m/s having a higher value than at the other velocity variations. This causes the tea particles to be easily lifted when the velocity inlet is higher. At 2.3 m/s, these solid particles more rapidly evaporated due to the number of solid volume fractions that were reduced more than the previous velocity.

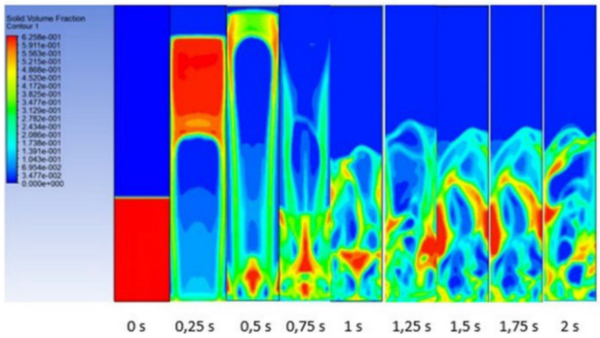

Fig. 6: 2D solid volume fraction at 1.8m/s.

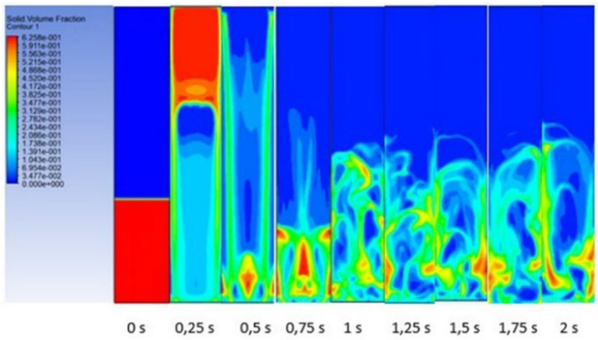

Fig. 7: 2D solid volume fraction at 2.1m/s.

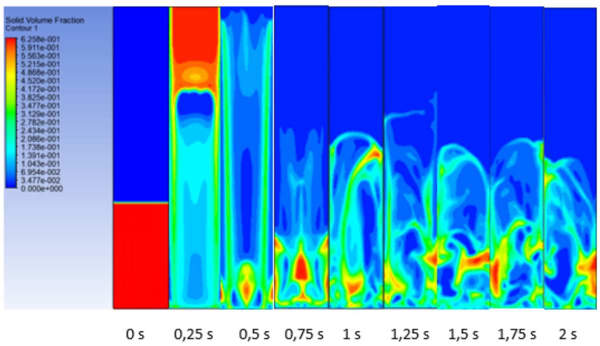

Fig. 8: 2D solid volume fraction at 2.3m/s.

Under the assumption of a fixed inlet area, a rise in air inlet velocity leads to a subsequent increase in flow rate. This elevated airflow rate improves the fluidization of particles, thereby promoting heightened contact among the particles and between the particles and the walls[33].

3.2 Pressure Drop

The fluidized state was primarily indicated by changes in the pressure drop across the bed layer[34]. There are several parameters that can affect the fluctuation of the pressure drop ratio, such as the increase in circulation flow[35], the number of particles added, and particle settling velocity[36]. An increase in velocity inlet in a fluidized bed dryer will affect pressure drop, as in Eq. 12. This correlation causes the pressure drop (ΔP) to increase linearly due to the velocity. Figure 9 shows the drop value of the pressure with the velocity of inlet air variation on the FBD. The drop of the pressure escalated with the fluidization velocity increase.

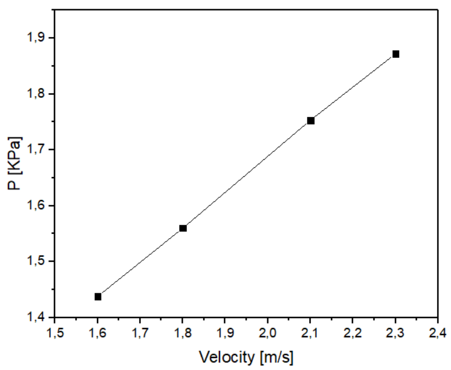

Fig. 9: Pressure drop on fluidized bed dryer.

3.3 Effect of Velocity Inlet on Heat and Mass Transfer

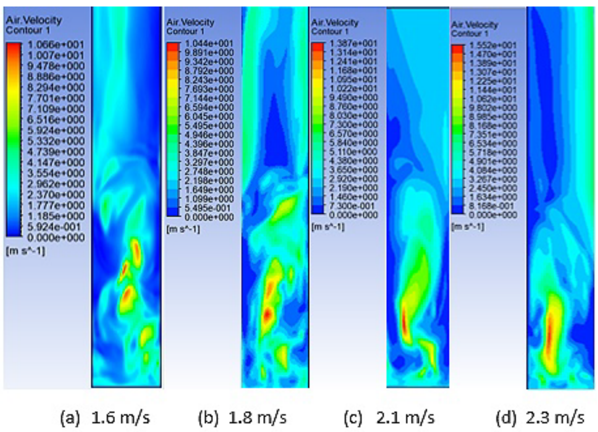

Fig. 10: Velocity distribution contour.

The temperature distribution contributes to the heat transfer within the particles. Figure 10 illustrates the contour of the magnitude of the inlet velocity, influencing the temperature distribution within the fluidized bed dryer. The inlet velocity impacts both the particle velocity and the velocity vector of particles. A lower velocity results in a diminished value of the particle velocity vector, consequently leading to reduced convection heat transfer on the particles.

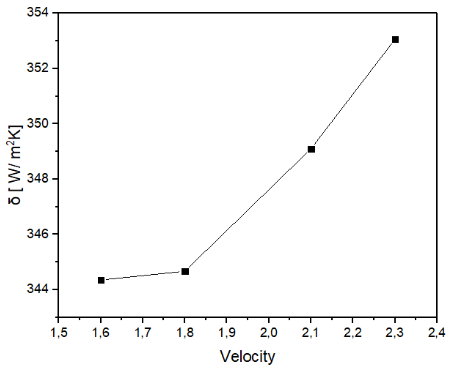

Fig. 11: Heat transfer coefficient between gas and solid.

Figure 11 illustrates that an increased fluidization velocity corresponds to higher transfer of the heat from the tea particles to the air. This is due to the greater air volume fraction when the fluidization velocity is getting higher. It corresponds to the correlation with the method of thermal Gunn[24] used in the analysis. Meanwhile, Fig. 12 illustrates that the heat transfer between the wall and solid particles intensifies with an increase in fluidization velocity. This phenomenon is attributed to the larger inlet velocity values, which elevate the volume fraction, consequently enhancing the heat transfer coefficient.

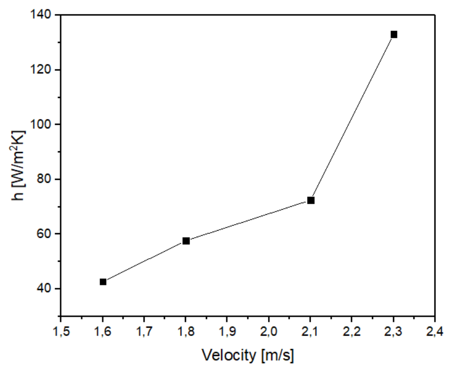

Fig. 12: Heat transfer coefficient between wall and solid.

The coefficient of heat transfer experiences an escalation with the increase in inlet velocity. In this study, the value of heat transfer between the air and the tea particles will be compared with the air volume fraction, as shown in Fig. 13. Observably, the heat transfer coefficient diminishes in regions characterized by an escalation in the air volume fraction. This phenomenon happens because the particle has lower resistance to heat transfer than the air. The viscous force causes the small value of air volume fraction of the wall at the no-slip condition of the airflow.

Figure 14 shows a radial profile of the tea particle temperature and the solid volume fraction for three-dimensional models at the height of 0.1 m. The elevation of the solid volume fraction induces a reduction in both particle velocity and granular temperature.

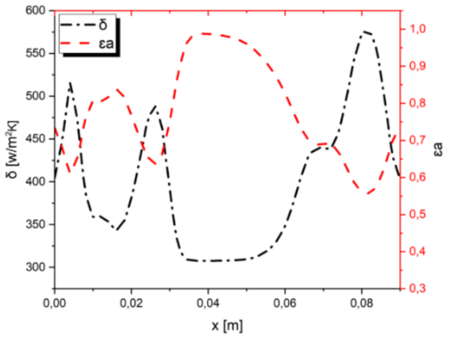

(a)

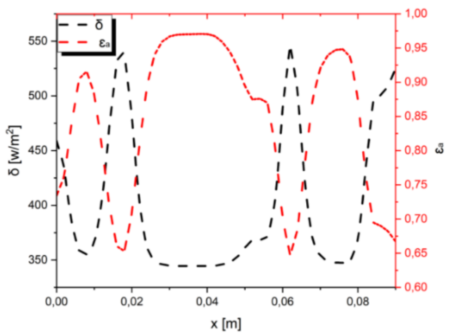

(b)

Fig. 13: Heat transfer coefficient on gas-solid and air volume fraction graph (a) at 1.6 m/s (b) at 2.3 m/s.

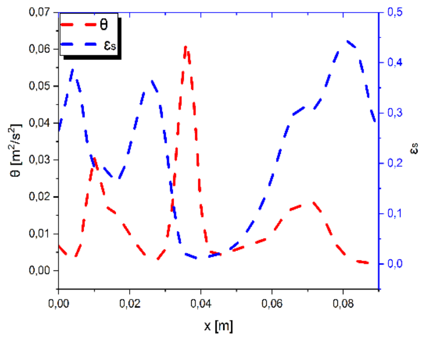

(a)

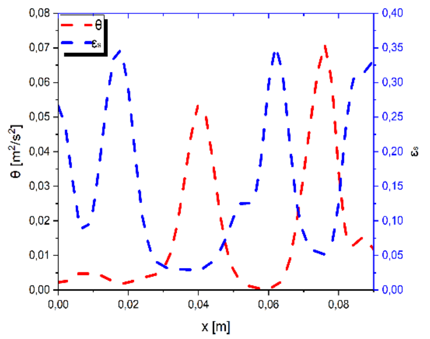

(b)

Fig. 14: Volume fraction and granular temperature graph (a) at 1.6 m/s (b) at 2.3 m/s.

Figure 15 shows the velocity distribution of particles at various velocity inlets at 0.1 m height. This value indicates that tea particle velocity elevated in the core of FBD and diminishes in the wall-close area. The corresponding profile elucidates a heightened tea particle volume fraction close to the wall and a deficiency in tea volume fraction around the center of the fluidized bed, as depicted in Fig. 13. This phenomenon occurs because the tea particle velocity on the wall has friction forces with the walls. As a result, the velocity of tea particles near the wall is diminished compared to the velocity of tea particles in the central region of the fluidized bed. This discrepancy contributes to an increased volume fraction of tea particles in the vicinity of the wall area.

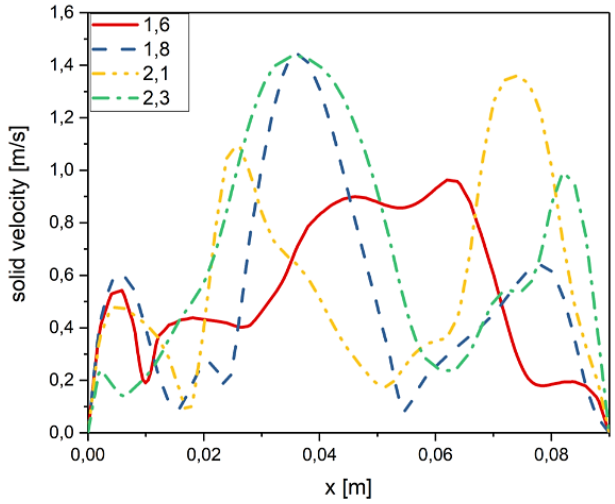

Fig.15: Tea particle velocity profile.

Table 2. Reynolds, Prandtl, and Sherwood number.

Velocity	Reynolds	Prandtl	Sherwood
1.6	57.81	0.74772	86.51
1.8	65.03	0.74772	50.44
2.1	75.87	0.74772	48.01
2.3	83.10	0.74772	47.01

In this study, the fluid flow has a maximum Reynolds number at 83.10, which is less than 200, and the Prandtl number of the air is all the same at 0.74772, as shown in Table 2, so the Sherwood number (Sh) can be calculated with Eq. 17.

From the calculation, it is known at 1.6 m/s, the Reynolds number is 57.81, the Prandtl number is 0.74772, and the Sherwood number is 86.51, while at 2.3 m/s, the Reynolds number is 83.10, the Prandtl number is 0.74772, and the Sherwood number is 47.01. The velocity variation of 2.3 m/s has the lowest Sherwood number, which can be interpreted as an increase in the rate of mass diffusion. The coefficient of mass transfer exhibits a considerable magnitude when either the diffusion coefficient or the rate of mass diffusion is substantial. In this scenario, the rise in diffusivity is influenced by the air temperature. An escalation in the airflow rate results in a corresponding increase in air temperature. The graphical representation of the mass and heat transfer coefficients is depicted in Fig. 16.

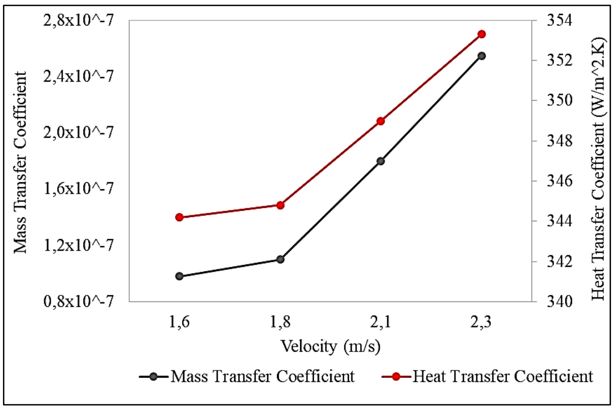

Fig. 16: Mass and heat transfer coefficient between gas and solid in air inlet velocity variation.

Figure 16 illustrates that there is a substantial increase in mass transfer when the fluidization velocity is elevated. At 1.6 m/s, the coefficient of the heat transfer is 344.2 $W/m^2.K$, and the coefficient of mass transfer is 0.98×10^{-7}, while at 2.3 m/s, the coefficient of the heat transfer is 353.3 $W/m^2.K$ and the coefficient of mass transfer is 2.55×10^{-7}. These values indicates that increasing the inlet air velocity maximizes the utilization of heat from the drying air. In the context of this study, it is noteworthy that despite maintaining a consistent drying air temperature at 403 K, distinct heat and mass transfer values were obtained.

Increasing the mass flow rate corresponds to an increase in the resultant heat transfer rate[37]). The findings in this study align with this principle, as demonstrated by the positive correlation observed between the velocity of the inlet air and the coefficient of heat transfer. This relationship is proportional to the escalation in mass flow rate, under the assumption of a constant inlet area. Consequently, it can be inferred that tea drying rates are accelerated with higher air velocities. This phenomenon is attributed to the escalation in air velocity within the fluidized bed, resulting in heightened mass and heat transfer rates. Consequently, this acceleration can expedite the process of tea drying. At the same drying air temperature, an increased air velocity facilitates an improved mass transfer process. This enhancement contributes to achieving a superior degree of dryness in the tea without necessitating a higher temperature which can damage the organic content in the tea leaves.

4. Conclusion

Fluidized bed dryers are widely applied in the industries such as mining and pharmaceuticals. Fluidized bed dryers are commonly used in the process of drying solid objects since it has a large heat and mass transfer rate that can reduce drying time. The value of inlet velocity influences the coefficients of the mass and heat transfer that occur in the FBD. Qualitative simulation results which describe the characteristics of the flow that occurs in the fluidized bed dryer due to variations in air inlet velocity can be seen in the 2D solid fraction contour. In this context, it is evident that with an increase in air inlet velocity, particles undergo a more rapid and elevated ascent during the rising stage. This is due to micro bubbles, which are formed at the base of the plate bed, having a high velocity so that when these bubbles gather, they will be able to lift the particles quickly and high. From the pressure drop result, it is known that the drop of the pressure escalated with the fluidization velocity increase.

From the results of the analysis, at 1.6 m/s, the coefficient of heat transfer is 344.2 $W/m^2.K$, and the coefficient of mass transfer is 0.98×10^{-7}, while at 2.3 m/s, the coefficient of heat transfer is 353.3 $W/m^2.K$ and the coefficient of mass transfer is 2.55×10^{-7}, in conclusion, an increase in the air velocity within the fluidized bed leads to an increase in both heat and mass transfer rates, thereby speed up the tea drying process. The elevation in both coefficient of the mass and the heat transfer can be attributed to the temperature distribution exhibited by the tea particles.

This research only focuses on the influence of the inlet air velocity on the flow characteristics that are formed, and this study does not carry out further on how the flow characteristics can occur if the inlet velocity becomes too high. To be directly implemented in the tea drying process, further studies can be carried out in the future to find out whether there are different flow characteristics or a critical turning point when the inlet air velocity becomes too high. This further research can also be related to fluidization efficiency. In summary, the Fluidized Bed Dryer (FBD) configuration with this velocity and temperature can effectively dry tea products. This process ensures the preservation of organic content quality in the tea while achieving an optimal dryness level suitable for storage purposes.

Acknowledgements

This work is supported and funded by “Riset Publikasi Internasional(RPI) Selain Anggaran Pendapatan dan Belanja Negara - II Batch” of Diponegoro University, Indonesia.

Nomenclature

v	velocity ($m\ s^{-1}$)
T	temperature (K)
Sc	Schmidt number (-)
S	surface area (m^2)
P	pressure (Pa)
L	height (m)

I	inertia (-)
g_o	radial distribution defined by Eq. 14
e	coefficient of restitution (-)
d_s	particle diameter (m)

Greek symbols

α	interphase drag coefficient (-)
δ	heat transfer coefficient (W m^{-2} K^{-1})
ε	volume fraction (-)
Θ	granular temperature (m^2 s^{-2})
μ	viscosity, shear stress (N s m^{-1})
ρ	density (kg m^{-3})
τ	Reynolds tensor stress (N m^{-2})

Subscripts

s	solid
mf	minimum fluidizng
kin	kinetic
g	gas
fr	friction
col	collision
a	air

References

1) S. Hanif, M. Sultan, T. Miyazaki, dan S. Koyama, “Steady-state investigation of desiccant drying system for agricultural applications,” *Evergreen*, **5** (*1*) 33–42 (2018). doi:10.5109/1929728.
2) K. Teshome, “Effect of tea processing methods on biochemical composition and sensory quality of black tea (camellia sinensis (l.) o. kuntze): a review,” *J. Hortic. For.*, **11** (*6*) 84–95 (2019). doi:10.5897/JHF2019.0588.
3) R. Cocco, S.B.R. Karri, dan T. Knowlton, “Introduction to fluidization,” *Chem. Eng. Prog.*, **110** (*11*) 21–29 (2014).
4) R.U. Rani, J.R. Banu, D.C.W. Tsang, dan C.H. Lay, “Thermochemical conversion of food waste for bioenergy generation,” INC, 2020. doi:10.1016/B978-0-12-818353-3.00005-5.
5) Y. Gunawan, N. Putra, E. Kusrini, I.I. Hakim, dan M.D.H. Setiawan, “Study of heat pipe utilizing low-temperature geothermal energy and zeolite-a for tea leaves withering process,” *Evergreen*, **7** (*2*) 221–227 (2020). doi:10.5109/4055223.
6) H. Bi, P. Jia, K. Qin, L. Yu, C. Cao, dan Y. Bai, “Optimization design of pot slot structure of tea de-enzyming and carding machine,” *Agronomy*, **12** (*12*) (2022). doi:10.3390/agronomy12122937.
7) S. Kavish, W.S. Botheju, dan C.S. De Silva, “Impact of inlet drying temperature in endless chain pressure dryers on the quality characteristics of leafy type of tea produced using different leaf standards,” *OUSL J.*, **10** (*0*) 73 (2016). doi:10.4038/ouslj.v10i0.7336.
8) R. Sivakumar, R. Saravanan, A. Elaya Perumal, dan S. Iniyan, “Fluidized bed drying of some agro products - a review,” *Renew. Sustain. Energy Rev.*, **61** 280–301 (2016). doi:10.1016/j.rser.2016.04.014.
9) X. Li, Y. Liu, T. Wang, N. Li, dan T. Zhang, “Experimental and numerical investigations on the hydrodynamics of gas-solid fluidized bed with an inclined agitator,” *Powder Technol.*, **380** 26–38 (2021). doi:10.1016/j.powtec.2020.11.054.
10) D.J. Patil, J. Smit, M. Van Sint Annaland, dan J.A.M. Kuipers, “Wall-to-bed heat transfer in gas-solid bubbling fluidized beds,” *AIChE J.*, **52** (*1*) 58–74 (2006). doi:10.1002/aic.10590.
11) A. Bakshi, C. Altantzis, R.B. Bates, dan A.F. Ghoniem, “Eulerian-eulerian simulation of dense solid-gas cylindrical fluidized beds: impact of wall boundary condition and drag model on fluidization,” *Powder Technol.*, **277** 47–62 (2015). doi:10.1016/j.powtec.2015.02.056.
12) A. Schmidt, dan U. Renz, “Numerical prediction of heat transfer between a bubbling fluidized bed and an immersed tube bundle,” *Heat Mass Transf. und Stoffuebertragung*, **41** (*3*) 257–270 (2005). doi:10.1007/s00231-004-0510-z.
13) N.H. Dong, L.M. Armstrong, S. Gu, dan K.H. Luo, “Effect of tube shape on the hydrodynamics and tube-to-bed heat transfer in fluidized beds,” *Appl. Therm. Eng.*, **60** (*1–2*) 472–479 (2013). doi:10.1016/j.applthermaleng.2012.08.018.
14) R. Yusuf, B. Halvorsen, dan M.C. Melaaen, “An experimental and computational study of wall to bed heat transfer in a bubbling gas-solid fluidized bed,” *Int. J. Multiph. Flow*, **42** 9–23 (2012). doi:10.1016/j.ijmultiphaseflow.2012.01.003.
15) T. Li, dan Y. Xu, “Computational fluid dynamics and its application to fluidization,” *Essentials Fluid. Technol.*, 109–129 (2020). doi:10.1002/9783527699483.ch6.
16) A.R.A. Bahar, A.S. Yatim, dan E.P. Wijaya, “CFD analysis of universitas indonesia psychrometric chamber air loop system,” *Evergreen*, **9** (*2*) 465–469 (2022). doi:10.5109/4794173.
17) A. Schmidt, dan U. Renz, “Eulerian computation of heat transfer in fluidized beds,” *Chem. Eng. Sci.*, **54** (*22*) 5515–5522 (1999). doi:10.1016/S0009-2509(99)00298-5.
18) K. Chen, P. Bachmann, A. Bück, M. Jacob, dan E. Tsotsas, “CFD simulation of particle residence time distribution in industrial scale horizontal fluidized bed,” *Powder Technol.*, **345** 129–139 (2019). doi:10.1016/j.powtec.2018.12.086.
19) L.M. Armstrong, S. Gu, dan K.H. Luo, “Study of wall-to-bed heat transfer in a bubbling fluidised bed using the kinetic theory of granular flow,” *Int. J. Heat Mass Transf.*, **53** (*21–22*) 4949–4959 (2010). doi:10.1016/j.ijheatmasstransfer.2010.05.047.

20) H.M. Abdelmotalib, dan I.T. Im, "Three dimensional modeling of heat transfer and bed flow in a conical fluidized bed reactor," *Int. J. Heat Mass Transf.*, **106** 1335–1344 (2017). doi:10.1016/j.ijheatmasstransfer.2016.10.117.
21) M. Upadhyay, A. Kim, H. Kim, D. Lim, dan H. Lim, "An assessment of drag models in eulerian–eulerian cfd simulation of gas–solid flow hydrodynamics in circulating fluidized bed riser," *ChemEngineering*, **4** (*2*) 1–19 (2020). doi:10.3390/chemengineering4020037.
22) S. Gosavi, N. Kulkarni, C.S. Mathpati, dan D. Mandal, "CFD modeling to determine the minimum fluidization velocity of particles in gas-solid fluidized bed at different temperatures," *Powder Technol.*, **327** 109–119 (2018). doi:10.1016/j.powtec.2017.12.026.
23) Y. Zhao, X. Shi, C. Wang, X. Lan, dan J. Gao, "Study on flow characteristics of turbulent fluidized bed with variable gas velocity due to chemical reactions," *Powder Technol.*, **416** (*January*) (2023). doi:10.1016/j.powtec.2022.118211.
24) D.J. Gunn, "Transfer of heat or mass to particles in fixed and fluidised beds," *Int. J. Heat Mass Transf.*, **21** (*4*) 467–476 (1978). doi:10.1016/0017-9310(78)90080-7.
25) A. Vepsäläinen, "Heterogeneous mass transfer in fluidized beds by computational fluid dynamics," 2014.
26) B. Lv, X. Deng, C. Shi, dan C. Fang, "Effect of agitation on hydrodynamics and separation performance of gas–solid separation fluidized bed," *Powder Technol.*, **388** 129–138 (2021). doi:10.1016/j.powtec.2021.04.084.
27) D.A. Wulandari, M. Akmal, Y. Gunawan, dan Nasruddin, "Cooling improvement of the it rack by layout rearrangement of the a2 class data center room: a simulation study," *Evergreen*, **7** (*4*) 489–499 (2020). doi:10.5109/4150468.
28) E. Yohana, M. Tauviqirrahman, A.R. Putra, A.E. Diana, dan K.H. Choi, "Numerical analysis on the effect of the vortex finder diameter and the length of vortex limiter on the flow field and particle collection in a new cyclone separator," *Cogent Eng.*, **5** (*1*) 1–15 (2018). doi:10.1080/23311916.2018.1562319.
29) S. Darmawan, K. Raynaldo, dan A. Halim, "Investigation of thruster design to obtain the optimum thrust for rov (remotely operated vehicle) using cfd," *Evergreen*, **9** (*1*) 115–125 (2022). doi:10.5109/4774224.
30) N. Hossain, dan R. Metcalfe, "Performance analysis of a 2d numerical model in estimating minimum fluidization velocity for fluidized beds," *Particuology*, **77** (2022). doi:10.1016/j.partic.2022.08.003.
31) Y. Zhang, J. Zhang, Y. Zhao, X. Zhang, X. Yang, E. Zhou, C. Duan, G. Wang, dan L. Dong, "Investigations on dynamics of bubble in a 2d vibrated fluidized bed using pressure drop signal and high-speed image analysis," *Chem. Eng. J.*, **395** (*December 2019*) (2020). doi:10.1016/j.cej.2020.125129.
32) J. Huang, R. Wang, R. Xu, B. Wu, D. Wang, Y. Liu, dan S. Zhang, "Numerical simulation of dynamic variation characteristics of particles in a rolling fluidized bed," *Processes*, **11** (*6*) (2023). doi:10.3390/pr11061696.
33) F. Jiang, X. Dong, G. Qi, P. Mao, J. Wang, dan X. Li, "Heat-transfer performance and pressure drop in a gas-solid circulating fluidized bed spiral-plate heat exchanger," *Appl. Therm. Eng.*, **171** (*February*) 115091 (2020). doi:10.1016/j.applthermaleng.2020.115091.
34) B. Lv, Z. Luo, B. Zhang, Y. Zhao, dan Y. Qin, "Fluidization characteristics and separation performance of mild-hot gas-solid fluidized bed," *Physicochem. Probl. Miner. Process.*, **55** (*1*) 184–195 (2019). doi:10.5277/ppmp18120.
35) S. Lv, F. Jiang, G. Qi, X. Chen, dan X. Li, "Pressure drop of liquid–solid two-phase flow in a down-flow circulating fluidized bed," *Powder Technol.*, **375** 136–145 (2020). doi:10.1016/j.powtec.2020.07.077.
36) J. Feng, Y. Shaokang, Q. Guopeng, dan L. Xiulun, "Particle distribution and pressure drop in a horizontal two-pass liquid-solid circulating fluidized bed," *Powder Technol.*, **416** (2023). doi:10.13353/j.issn.1004.9533.20200324.
37) A.S. Pamitran, S. Novianto, dan A.S. Santoso, "Intermittent flow pattern on two phase flow boiling with horizontal microchannel," *Evergreen*, **7** (*1*) 150–154 (2020). doi:10.5109/2740972.